IN-FLIGHT CALIBRATION OF THE INTUITIVE MACHINES IM-1 OPTICAL NAVIGATION IMAGERS

John Y Pelgrift[*], Derek S Nelson[*], Coralie D Adam[*], Giovanni Molina[†], Michael Hansen[†], Andrew Hollister[†]

Accurate camera calibration is critical for any optical navigation system that uses imagery taken from the spacecraft to estimate its position and especially for onboard autonomous navigation systems that need to work without human intervention. Intuitive Machines' IM-1 mission presented several unique challenges for camera calibration, including a very short 7-day mission, a commercial off-the-shelf lens with unknown characteristics, and a camera filter that prevented imaging all but the brightest stars (m $<$ 3.5). This paper presents the pre-flight preparations and the in-flight results of the IM-1 camera calibration campaign.

INTRODUCTION

Intuitive Machines' IM-1 mission launched on February 15, 2024, and landed on the surface of the Moon seven days later on February 22, 2024. Critical to the successful lunar landing was Intuitive Machines' onboard optical navigation and hazard detection software,[1, 2, 3] which utilized two cameras onboard the spacecraft: the Terrain Relative Navigation (TRN) camera and the Hazard Relative Navigation (HRN) camera. These two cameras, whose design specifications are detailed in Table 1, use the same CMOS detector but have different optics designs, optimized to each camera's specific use case. Like all optical navigation cameras, these cameras required calibration to enable accurate navigation from the measurements derived from their imagery. This includes calibration of each camera's optical distortion model and each camera's frame alignment with respect to the spacecraft. These calibrations are accomplished by acquiring images of star fields with the cameras, observing the locations of the stars in the images, and then estimating the camera attitude and camera model parameters by fitting, in a least-squares sense, the observed star locations to the star locations predicted using a star catalog. Many previous descriptions and reports of such stellar camera calibrations are documented in prior literature.[4, 5, 6, 7] Image processing and camera calibration estimation was performed using the KinetX Image Processing Python library (KXIMPy), which itself utilizes NASA's GIANT optical navigation library.[8, 9] This paper details the results of the in-flight calibration campaign using stellar imagery for the two optical navigation cameras, as well as the calibration preparation, planning, and analysis conducted pre-flight.

The OpenCV (Brown) camera model with a temperature-dependent focal length was used to model the geometric distortion of both cameras, as described by the following equations:[10]

$$\begin{bmatrix} x' \\ y' \end{bmatrix} = \frac{1}{z} \begin{bmatrix} x \\ y \end{bmatrix}$$

$$r^2 = x'^2 + y'^2$$

$$\begin{bmatrix} x'' \\ y'' \end{bmatrix} = (1 + k_1 r^2 + k_2 r^4 + k_3 r^6) \begin{bmatrix} x' \\ y' \end{bmatrix} + \begin{bmatrix} 2p_1 x' y' + p_2(r^2 + 2x'^2) \\ p_1(r^2 + 2y'^2) + 2p_2 x' y' \end{bmatrix}$$

[*]Space Navigation and Flight Dynamics Practice, KinetX, Inc., 21 W. Easy Street Ste. 108, Simi Valley, CA 93065
[†]Intuitive Machines, 13467 Columbia Shuttle Street, Houston, TX 77059.

$$\begin{bmatrix} u \\ v \end{bmatrix} = \begin{bmatrix} f_x(1+a_1T) & 0 & c_x \\ 0 & f_y(1+a_1T) & c_y \end{bmatrix} \begin{bmatrix} x'' \\ y'' \\ 1 \end{bmatrix}$$

where $[x, y, z]$ is a pointing vector in the camera frame, k_1, k_2, and k_3 model the radial distortion, p_1 and p_2 model the tangential or "tip/tilt" distortion, f_x and f_y are the focal length in units of pixels in the two image directions, a_1 models the temperature dependence of the focal length, T is the camera temperature in degrees Celsius, and $[u, v]$ is the resulting projected image location.

Table 1. TRN and HRN nominal (design) camera parameters

Parameter	TRN	HRN
Focal length [mm]	6.5	16.2
Aperture diameter [mm]	0.8125	1.2
Aperture F#	F/8	F/13.5
Horizontal FOV [°]	47.35	19.96
Vertical FOV [°]	36.45	15.05
Diagonal FOV [°]	57.47	24.81
Sensor size [pixels]	2592 x 1944	
Sensor size [mm]	5.7 x 4.28	
Pixel pitch [mm]	0.0022 x 0.0022	

The IM-1 mission presented several limitations and challenges to the in-flight calibration effort. The primary limitation involved the HRN camera, which included a fixed filter that significantly reduced the amount of light reaching the detector. This meant that even when using the camera's maximum exposure time and gain, the limiting stellar magnitude was predicted to only be ∼3.5–4. This low limiting magnitude made it very difficult to image enough stars for an effective calibration and necessitated careful planning of the calibration attitude targets to capture star fields that would be visible with this camera while simultaneously meeting several other spacecraft attitude constraints.

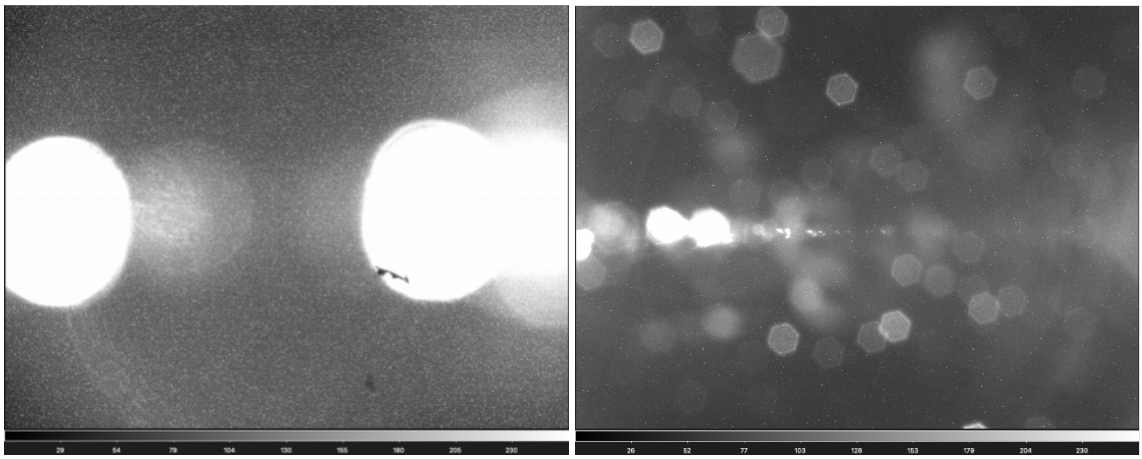

Figure 1. Example calibration images captured in-flight with the HRN camera (left) and TRN camera (right), showing significant scattered light reflected off of the spacecraft's landing legs.

In addition, the mission's seven day transit provided limited time to complete the imaging activity onboard, downlink the images, perform the camera calibration on the ground, and then uplink the calibration products back to the spacecraft before they were needed by the onboard optical navigation software. Multiple tests and rehearsals were conducted pre-launch to develop and improve the processes, interfaces, and tools required to

enable a successful in-flight calibration within such a short time period. However, the compressed timeline allowed very little margin to react to anomalies experienced in-flight and also meant that the data downlink budget was very tight, which significantly limited the number of calibration images that could be downlinked and processed.

Finally, when the images were downlinked in-flight, they showed unexpected and severe scattered light, shown in Figure 1, coming from sunlight reflected off the spacecraft's landing legs which significantly degraded the image data quality and obscured stars. Additionally, attitude error with respect to the intended targets meant that the intended star fields for the HRN camera were not fully captured. These two factors limited the number of observable stars in the images, especially for the HRN camera. In rapid response, we developed techniques to attempt to correct the image data and extract as much usable information from the images as possible, resulting in a partially successful camera calibration.

ATTITUDE TARGET PLANNING

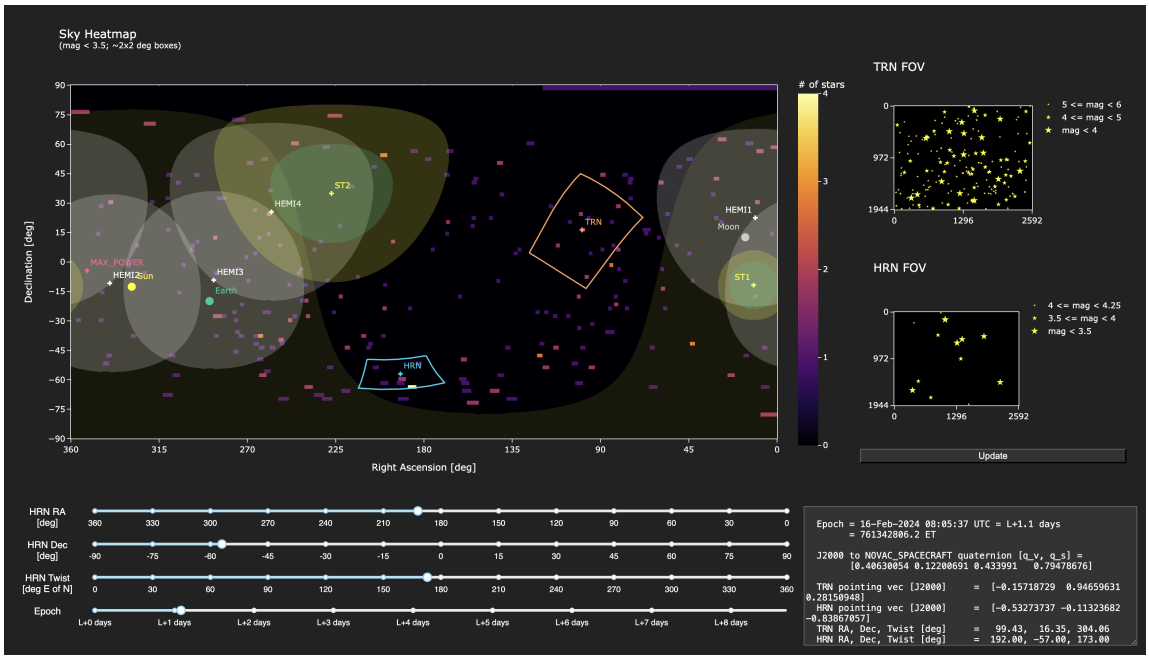

Figure 2. Screenshot of the attitude target planning tool developed to select star fields for calibration images while visualizing other spacecraft attitude constraints. Shown is attitude target #2 that was used for the in-flight calibration (see Table 2).

Planning the in-flight calibration imaging activity required carefully selecting spacecraft attitudes where both cameras could see an adequate star field, while also simultaneously meeting several other spacecraft attitude requirements. These requirements included keeping both cameras >90 degrees from the Sun to reduce stray light in the images, keeping the Earth <45 degrees from at least one of the spacecraft's four hemispherical antennas to maintain communication with the spacecraft during the imaging activity, keeping the Sun and Earth out of the respective keep out zones of the spacecraft's two star trackers to maintain attitude knowledge, and keeping the Earth and Moon out of the cameras' fields of view (FOV).

To find spacecraft attitudes that met all of these constraints at once, we developed an interactive tool, shown in Figure 2, for visualizing all of the relevant spacecraft components and solar system bodies on a heat map of the sky that shows the locations of stars of magnitude 3.5 or brighter. The bright star heat map facilitated targeting an adequate star field for the HRN camera while the other overlaid visualizations showed if the rest of the requirements were also being met. The low limiting magnitude of the HRN camera made it difficult to find star field targets that would include any more than a few stars visible to that camera. The process

Table 2. Calibration attitude targets selected for IM-1 (15 Feb 2024 launch date)

Parameter	Requirement	Target 1	Target 2
HRN (RA, Dec, Twist) [°]	Visible stars	(82.00, 39.00, 52.00)	(192.00, -57.00, 173.00)
TRN (RA, Dec, Twist) [°]	Visible stars	(99.43, 16.35, 304.06)	(220.89, 25.36, 121.71)
TRN Sun angle [°]	>90	111.54	131.99
HRN Sun angle [°]	>90	115.72	101.87
TRN Earth angle [°]	Outside FOV	80.45	169.92
HRN Earth angle [°]	Outside FOV	149.70	77.27
TRN Moon angle [°]	Outside FOV	135.03	80.13
HRN Moon angle [°]	Outside FOV	63.39	135.50
Minimum antenna angle to Earth [°]	<45	4.26	10.93
Star Tracker 1 Sun angle [°]	>17.5	24.64	41.98
Star Tracker 2 Sun angle [°]	>45	117.74	106.81
Star Tracker 1 Earth angle [°]	>12	38.50	79.16
Star Tracker 2 Earth angle [°]	>25	110.01	80.56

generally involved scanning the HRN FOV across the sky to search for clusters of bright stars and then looking for a twist (roll about the camera boresight) angle that would allow all the other constraints to be met. This process was then repeated for each launch date within a given window each time the launch window slipped. Despite the many attitude constraints, this tool allowed us to select targets for each launch date, including the two attitude targets that were used in-flight. These two targets, detailed in Table 2, each included six stars <3.5 magnitude in the HRN field of view while also meeting the other attitude requirements.

GROUND TESTING AND REHEARSALS

Thermal Testing

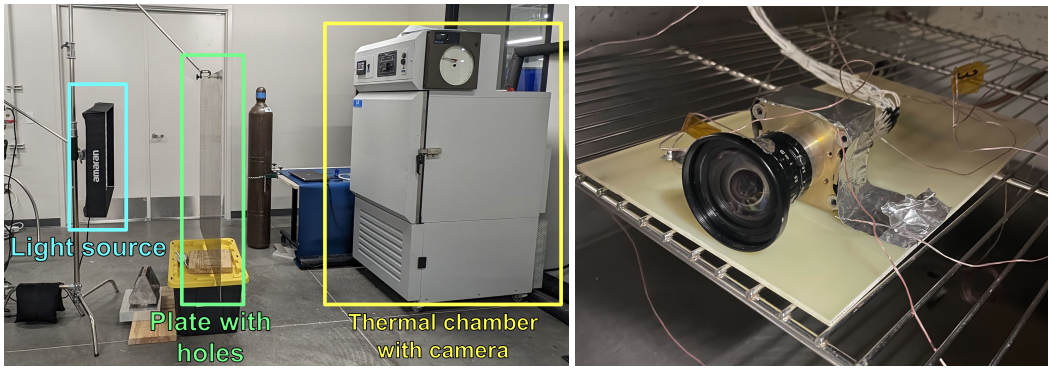

Figure 3. (Left) Test setup for the thermal imaging analysis used to attempt to evaluate the temperature dependence of the camera model. (Right) The TRN camera EDU inside the thermal chamber with temperature sensors attached.

Several ground tests were completed pre-launch to evaluate and analyze the cameras and to rehearse the processes and procedures of the in-flight calibration. The limiting magnitude of each camera when using its maximum exposure time was initially unknown, so night sky testing (taking images of the stars of the night sky from the ground) was used to evaluate the dimmest stellar magnitude that each camera could observe. Night sky testing is limited by the atmosphere and light polution, however it helps inform the lower bound of the limiting magnitude. The temperature dependence of the camera models was also highly uncertain, especially for the TRN camera, which used a commercial off-the-shelf (COTS) lens for which no optical or thermal model was available.

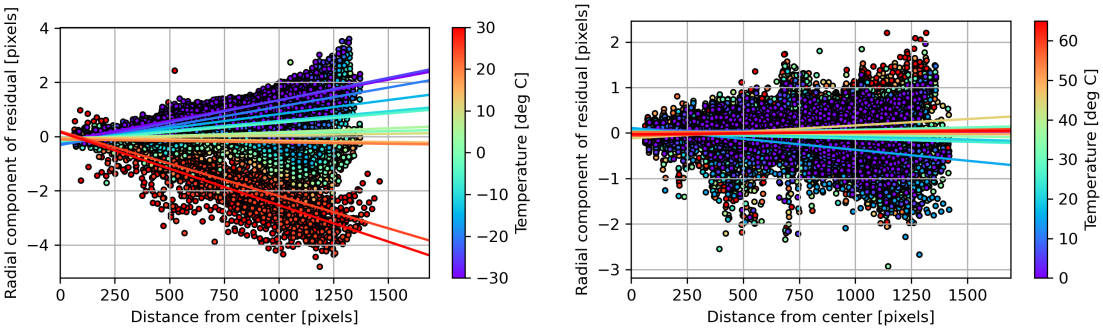

Figure 4. Results from the thermal tests for two of the test runs. Shown is the radial component of the residuals over the radial distance of the hole from the camera's principal point, colored by temperature and with a linear fit to each temperature.

We conducted multiple imaging tests with the camera in a thermal chamber, as seen in Figure 3, in an attempt to evaluate the temperature dependence of the TRN camera's focal length. These tests involved taking images of a back-lit steel plate with a uniform grid of small holes while the temperature of the camera was heated and cooled through a wide range of temperatures. The backlit holes appeared as point light sources in the image and could be detected with the same centerfinding techniques used to detect stars. Then the 3D positions of the holes with respect to the camera were modeled to create a "catalog" of hole positions, which could then be used, with the camera model, to predict where the holes should appear in the image. The observed and predicted hole locations could then be compared to look for changes as the temperature was varied. The 3D modeling of the hole locations was not high-fidelity, and as such, this test was only intended to look for relative changes in the focal length as the temperature varied and not to produce an absolute calibration of the camera.

This test was performed multiple times, and the results varied, as shown in Figure 4, and were therefore somewhat inconclusive. In a subset of the tests, an apparent temperature dependence was observed, while other tests showed no temperature dependence. We suspect that the camera was shifting slightly in between images when the door to the thermal chamber was opened and closed to take each image. The camera position was assumed to be constant during the test, so if the camera was moving towards or away from the plate in between images, it would have a similar effect as a change in focal length by causing the apparent image locations of the holes to move radially in or out from the image center. Nevertheless, the test results helped bound the temperature dependence we could expect to see in-flight and gave us confidence that we would not see a temperature dependence effect larger than a few pixels at most.

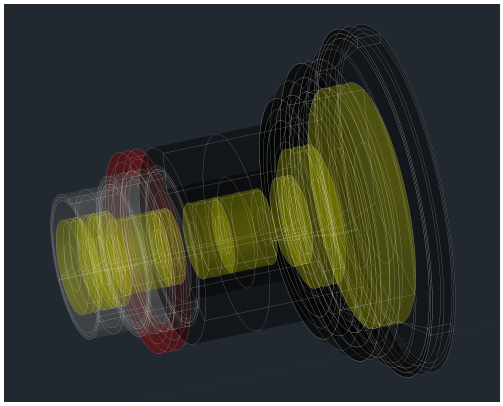

Figure 5. Improved TRN lens CAD model based on measurements of the EDU lens cut open by waterjet.

In addition, the Intuitive Machines thermal team conducted multiple thermal vacuum chamber tests with the camera to measure the thermal response of each component of camera as it was heated and cooled. They also cut open one of the TRN engineering design unit (EDU) lenses to precisely measure the internal components to improve the CAD and thermal models, as seen in Figure 5. These tests and the imaging tests helped improve the confidence in the thermal modeling and bound the temperature dependence of the camera focal length, however there was still uncertainty going into the mission due to the limitations in the testing setups.

Mission Sequence Tests

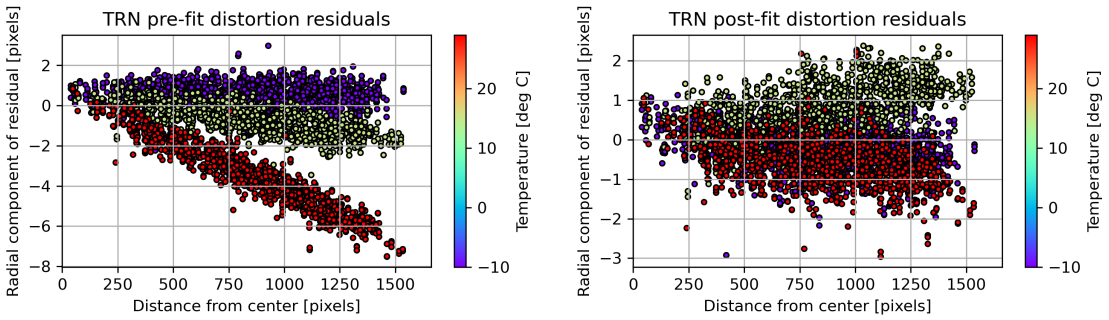

Figure 6. (Left) Radial component of the pre-fit TRN residuals from the mission sequence test (MST) showing a clear un-modeled temperature-dependence. (Right) the post-fit residuals after estimating a linear focal length temperature dependence, showing reduced error but some remaining mis-modeling.

In addition to ground tests of the camera hardware, multiple rehearsals of the in-flight calibration were conducted using simulated data to train the teams and refine the operations processes. These included a real-time test of the calibration imaging activity in isolation and a full mission sequence test (MST) from launch to lunar landing, which included rehearsing both the spacecraft operations for camera calibration imaging and the ground calibration data processing (using simulated images). These tests provided the various operations teams an opportunity to learn how to work together and smoothly exchange data and information, helped develop and refine the operations procedures and processes, and served as practice for processing the calibration imagery and producing the calibration data products.

The images for the MST were simulated using "truth" camera models, perturbed from the a priori models in a manner not disclosed to the team until after the conclusion of the test. The truth TRN model included a clear observable temperature dependence in the focal length with an effect of several pixels of error, as seen in Figure 6. This temperature dependence was mostly well estimated during the test, but some mis-modeling remained in the post-fit residuals. This indicated either a non-linear focal length temperature dependence and/or error in the temperature data used for each image. This scenario helped the team practice estimating a temperature-dependent focal length and working through the decision-making of such a scenario. The spacecraft's onboard flight software did not include the ability to model a temperature-dependent focal length, so a single constant focal length needed to be selected for uplink. In this scenario, the team decided to use the focal length estimated using only the hot images, but the scenario allowed the team to work through different options that could be exercised based on what the data looked like in-flight.

The truth HRN model included a slight temperature dependence in the focal length with an effect of only a few tenths of a pixel of error. With star centerfinding error on the same order, this level of temperature dependence would be just on the edge of what could be observed. During the test, the team did not observe any temperature dependence, however post-test analysis revealed that the iterative coadding technique implemented for HRN was introducing error and masking the effect. This test helped the team test out this technique and ultimately discover that it was flawed, as discussed in the following section.

IMAGE COADDING

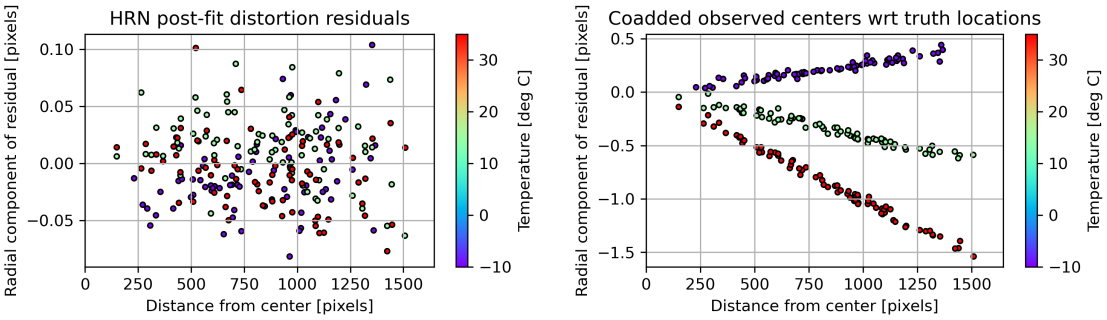

Figure 7. (Left) Post-fit calibration residuals using the iterative coadding with simulated data, which (falsely) indicated a good fit. (Right) Residuals showing the observed centers from the coadded images with respect to their truth locations, showing that the iterative coadding/calibration process had in fact introduced error.

Image coadding was explored pre-flight as a potential strategy to mitigate the HRN camera's low limiting magnitude by increasing the signal-to-noise ratio (SNR) of the stars in the images and allowing for additional stars to be observed below the single-image limiting magnitude. Since the camera model is itself used within the coadding process to register the images in the stack, the idea was to implement a process where the coadding and calibration were performed iteratively until convergence on a final camera model was achieved.

This idea was ultimately abandoned after tests with simulated data showed that this could produce erroneous results because there was nothing constraining the calibrated model to the original image data and the solution could walk away from the truth. Figure 7 shows results from one of these tests, where a small temperature dependence was added to the truth model for the simulation. The post-fit calibration residuals using the iterative coadding technique were zero-mean for all temperatures, which would indicate that the temperature dependence had been well modeled. However, when the star centers observed in the final coadded images were compared to the truth star locations, it could be seen that the iterative coadding/calibration process had actually introduced error. In fact, the final model estimated with this process had more error than the a priori model that was used.

We also explored the idea of doing image coadding without registering the images, which we determined would work if the camera attitude was very stable over the image set, but the attitude stability required was beyond the capabilities of the spacecraft's attitude control system.

IN-FLIGHT RESULTS

Flight operations for IM-1 were dynamic, and the imaging plan we had originally developed was adapted on-the-fly in response to an evolving spacecraft state. We had originally planned to take three image sets: one at cold temperatures (–10 to –5 deg C) at attitude target #1, one at warm temperatures (∼15 deg C) also at attitude target #1, and one at hot temperatures (∼30 deg C) at attitude target #2 (see Table 2 for attitude target details). Heaters were used to bring each camera up to the desired temperatures. The hot temperature was selected to roughly match the temperatures expected for the two cameras when they would be in use during the descent to the lunar surface. Each of these individual image sets was planned to include 25 HRN images and 3 TRN images.

Due to issues experienced in-flight, only two image sets, one at each attitude target, were acquired in the initial imaging activity intended to acquire all three. In addition, the TRN heater was unable to heat the camera to the desired temperatures despite it running for several hours, so both image sets were taken at cold temperatures between approximately –23 deg C and –11 deg C. The HRN heater worked as expected, so HRN images were captured at the intended warm and hot temperatures. In addition, the attitudes that the images were captured at were off from the intended targets by approximately 8.7 and 7.5 degrees respectively. This

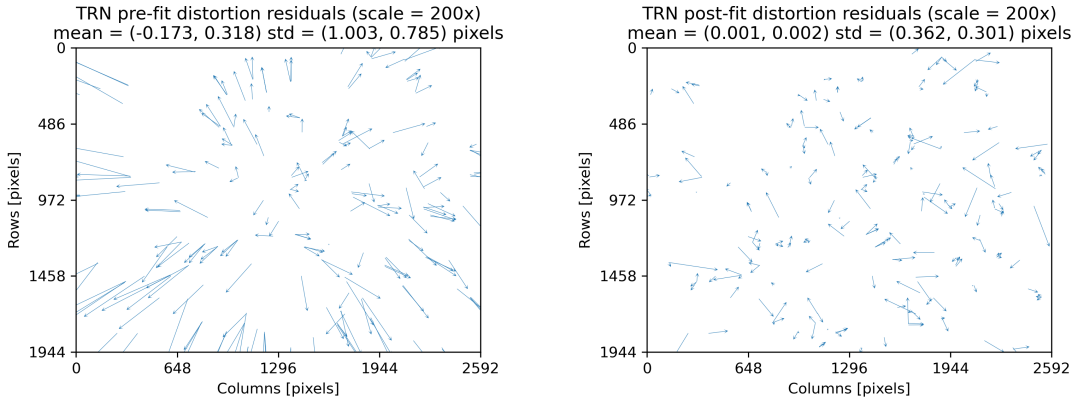

Figure 8. Pre-fit (left) and post-fit (right) calibration residuals for the TRN camera, showing the difference between predicted and observed star locations in the image before and after calibrating the camera's distortion model in-flight.

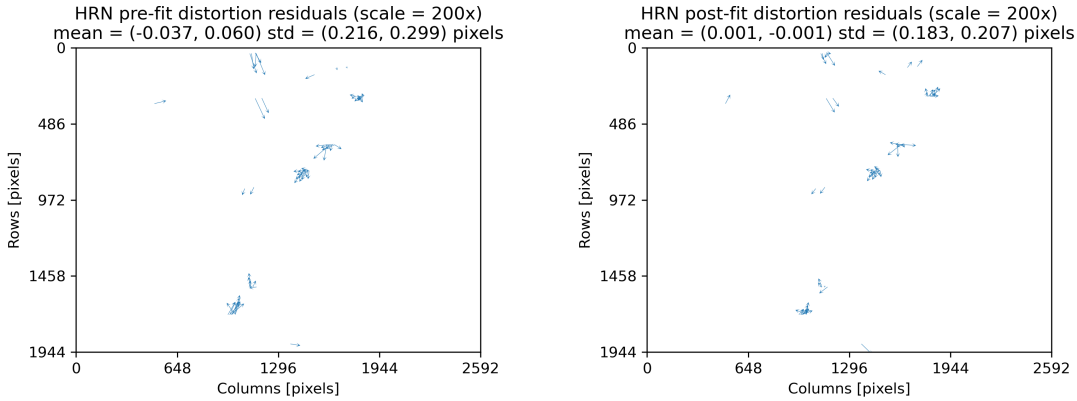

Figure 9. Pre-fit (left) and post-fit (right) calibration residuals for the HRN camera, showing the difference between predicted and observed star locations in the image before and after calibrating the camera's distortion model in-flight.

meant that the intended starfields for the HRN camera were not fully captured, and the number of stars visible with HRN was severely limited.

The two initial image sets were where the extreme stray light, shown in Figure 1, was observed. A third image set, for TRN only, was acquired later at the attitude that the spacecraft happened to be in at the time. This third TRN image set showed much less stray light. Later analysis revealed that the attitude they were taken at had the lander leg located under the TRN camera in shadow.

Spacecraft operations during the mission limited data downlink time available for calibration images. This meant that of the 59 total images taken for calibration, only 28 were eventually downlinked and used for the calibraiton (9 of 9 for TRN and 19 of 50 for HRN).

Hot pixel correction

The stray light observed in the first two image sets significantly increased the level of noise in the images and produced a substantial amount of hot pixels. In response to this, we developed a method to attempt to correct for and remove the hot pixels in the images to improve the data quality.

We began by using a technique used by others[11, 12] to remove the average background pattern of the stray light from each image with extreme stray light. This involves flattening each image by subtracting a 5x5 median filtered version of the image from itself. What is left should be only small point sources (stars) and hot pixels. To remove the stars and average out image-to-image noise and variation in the hot pixels, the flattened images were then stacked and the median of the stack was used as the "hot pixel map". For TRN, the attitudes were not varying enough for this coadding to completely remove stars, so we then applied a standard deviation filter, where any pixels with a standard deviation in the stack higher than 15 DN were set to zero in the hot pixel map. This helped avoid adding star signal to the map. This hot pixel map was then subtracted from each image to correct for the hot pixels.

Distortion calibration

Table 3. TRN and HRN camera distortion calibration results

Model	TRN			HRN		
parameter	A priori	Estimated	1σ Uncert.	A priori	Estimated	1σ Uncert.
f_x [pixels]	3020.418	3017.052	0.641	7276.777	7278.865	2.699
f_y [pixels]	3020.345	3017.022	0.602	7276.766	7279.034	1.551
k_1	-0.18043	-0.18210	1.33e-3	0.29764		
k_2	0.12505			-0.87209		
k_3	-0.045161			-47.004		
p_1	3.1460e-4	-5.6437e-5	1.24e-4	2.3107e-4		
p_2	-2.7356e-4	2.6303e-4	8.81e-5	7.7385e-4		
c_x [pixels]	1302.789			1271.447		
c_y [pixels]	912.780			981.483		
a_1 [1/°C]	0.0			0.0		

Parameters with no estimated value shown were not estimated due to lack of data (a priori value was used).

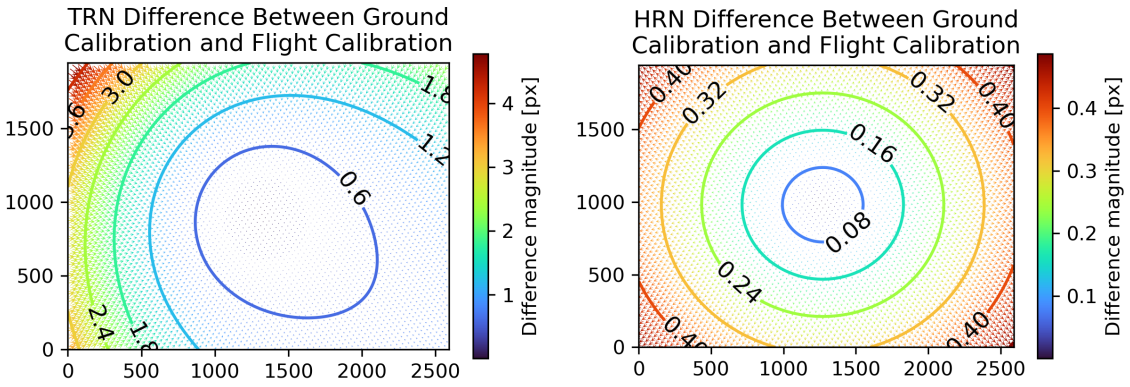

Figure 10. Projected differences between the a priori camera model (estimated during a ground calibration) and that estimated during the in-flight calibration for TRN (left) and HRN (right). These plots show the correction to each camera model that was made by the in-flight calibration.

For the HRN camera, which was significantly limited in the number of usable star observations, only the focal length was estimated, correcting ~0.4 pixels of error at the edges of the FOV with respect to the a priori model, as seen in Figures 9 and 10. The optical distortion terms of the model were not estimated for the HRN camera due to a lack of data. No temperature dependence was observed in the focal length over the

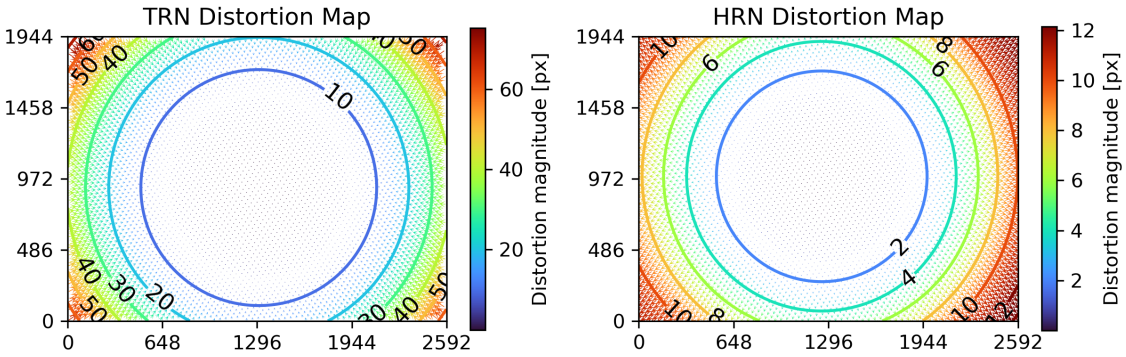

Figure 11. Distortion maps for TRN (left) and HRN (right). These maps show the effect of the distortion terms of the model with respect to the corresponding distortion-less pinhole camera models.

temperature range captured (roughly +17 deg C to +27 deg C), although this range was smaller than planned and only two stars were observed in the images at the colder temperatures.

For the TRN camera, which had many more usable star observations, both the camera focal length and the first order optical distortion terms were estimated, correcting ∼4 pixels of error in one corner of the FOV with respect to the a priori model, as seen in Figures 8 and 10. The corrections made were asymmetrical due to significant changes to the tip/tilt (p_1/p_2) terms of the model, as seen in Table 3. Like HRN, no temperature dependence was observed in the focal length of TRN, however all of the images were captured at much colder temperatures and across a smaller range than planned.

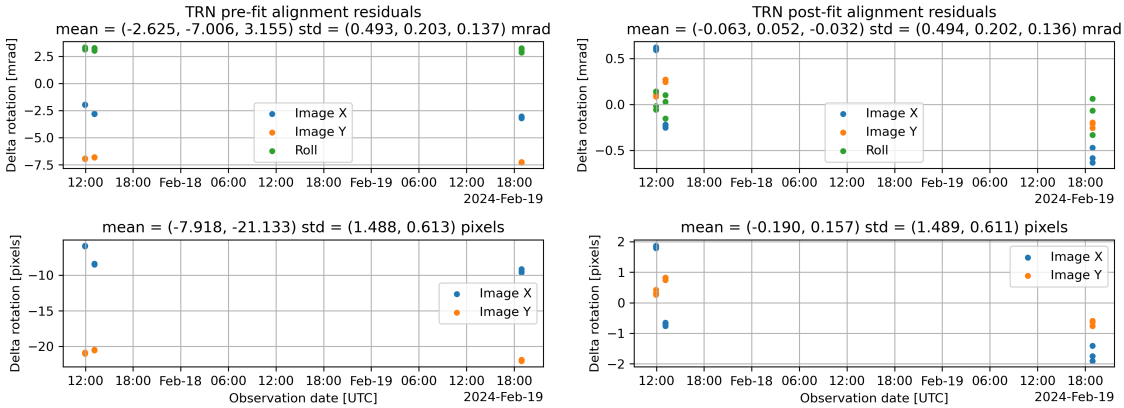

Figure 12. Pre-fit (left) and post-fit (right) alignment residuals for the TRN camera, showing the difference between the camera attitude predicted by the GNC-estimated spacecraft attitude plus the camera alignment and the observed camera attitude estimated using the stars in the image. These differences are expressed as Euler angles representing rotations corresponding to the two image coordinate directions and the roll about the camera boresight.

Figure 11 shows a map of the estimated distortion for each camera. These maps show, in units of pixels, the projected differences between the estimated camera model with distortion and the underlying pinhole camera model without distortion. TRN was estimated to have a maximum of 75 pixels of distortion at the corners of its FOV, and HRN was estimated to have a maximum of 12 pixels of distortion at the corners of its FOV.

Alignment calibration

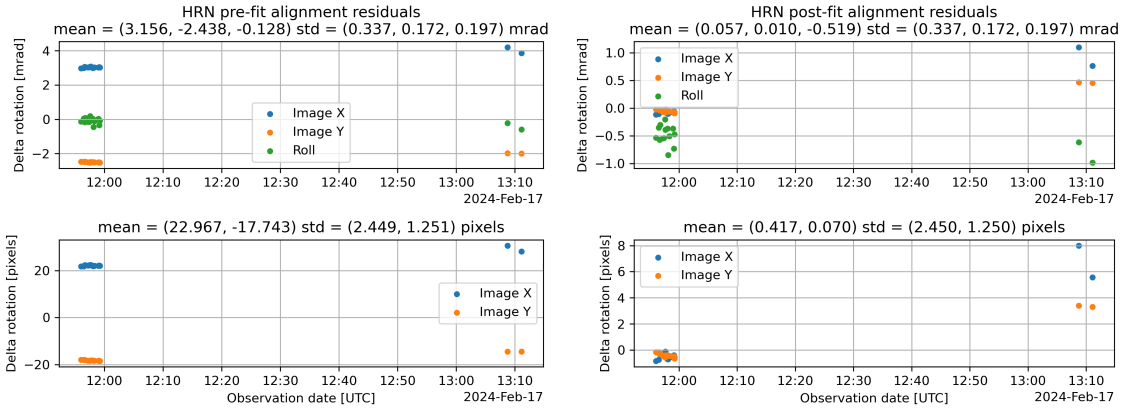

Figure 13. Pre-fit (left) and post-fit (right) calibration residuals for the HRN camera, showing the difference between the camera attitude predicted by the GNC-estimated spacecraft attitude plus the camera alignment and the observed camera attitude estimated using the stars in the image. These differences are expressed as Euler angles representing rotations corresponding to the two image coordinate directions and the roll about the camera boresight.

The camera frame alignment was also successfully estimated for both cameras, correcting roughly 24 and 10 arcmin of a priori alignment error for the TRN and HRN cameras respectively, as shown in Figures 12 and 13. Both cameras showed relatively large alignment differences (several pixels) between image sets. This was likely due to changing estimates of the star tracker alignments within the attitude estimation filter and should be corrected for the next IM-2 mission.

LESSONS LEARNED

Many lessons were learned through the planning and execution of the IM-1 in-flight camera calibration that will be applied to the follow-up IM-2 mission. The most significant was the planning difficulty caused by the very low limiting magnitude of the HRN camera. For IM-2 the filter on the HRN lens will be removed to allow significantly more light into the camera to improve the limiting magnitude and make attitude planning much easier. Second, the stray light observed reflecting off the landing legs degraded the image data. This will be primarily mitigated by adding a new baffle to each camera to reduce the light reflected off spacecraft components that can make it into the camera optics. As a backup mitigation method, specific calibration attitudes will be planned to shadow the legs under each of the cameras. Finally, the TRN camera heater did not work as intended to heat the TRN camera during the calibration activities. As a result, the heater design and thermal modeling will be re-visited and improved, to allow heating TRN to the desired operational temperatures during the calibration.

CONCLUSION

Despite the many challenges, a partially successful calibration was completed in-flight for both cameras. The extensive pre-flight testing and preparations maximized the chance of success in-flight, and when the in-flight data quality turned out to be poor, quick development of corrective techniques allowed for usable data to be extracted from the images and a calibration of both camera models and alignments was completed. The calibrated camera models and frame alignments were uplinked to the spacecraft and used by the onboard optical navigation and hazard avoidance algorithms during the descent to the lunar surface. Onboard optical navigation processing from the TRN and HRN cameras enabled the first successful landing on the Moon by a private company. While the calibration did not go fully as expected, the lessons learned from working through the issues we experienced are invaluable and will be crucial for the follow-up IM-2 mission.

REFERENCES

[1] J. A. Christian, L. Hong, P. McKee, R. Christensen, and T. P. Crain, "Image-Based Lunar Terrain Relative Navigation Without a Map: Measurements," *Journal of Spacecraft and Rockets*, Vol. 58, No. 1, 2021, pp. 164–181, 10.2514/1.A34875.

[2] G. Molina *et al.*, "Visual Odometry for Precision Lunar Landing," *Proceedings of the 44th Annual American Astronautical Society Guidance, Navigation, and Control Conference, 2022*, Springer International Publishing, 2024, pp. 1021–1042, 10.1007/978-3-031-51928-4_58.

[3] J. Getchius *et al.*, "HAZARD DETECTION AND AVOIDANCE FOR THE NOVA-C LANDER," *Proceedings of the 44th Annual American Astronautical Society Guidance, Navigation, and Control Conference, 2022* (M. Sandnas and D. B. Spencer, eds.), Springer International Publishing, 2024, pp. 921–943, 10.1007/978-3-031-51928-4_53.

[4] J. Y. Pelgrift *et al.*, "In-Flight Calibration of the OSIRIS-REx Optical Navigation Imagers," 1st Space Imaging Workshop, 2018.

[5] B. J. Bos, D. S. Nelson, J. Y. Pelgrift, *et al.*, "In-Flight Calibration and Performance of the OSIRIS-REx Touch And Go Camera System (TAGCAMS)," *Space Science Reviews*, Vol. 216, No. 4, 2020, p. 71, 10.1007/s11214-020-00682-x.

[6] E. Sahr, E. Lessac-Chenen, J. Pelgrift, D. Nelson, C. Adam, and D. Stanbridge, "Post-Launch Characterization and Calibration of the Optical Navigation Instruments for NASA's Lucy Mission," 3rd Space Imaging Workshop, 2022.

[7] Y. Zhao *et al.*, "Pre-flight and In-flight Calibration and Performance of the Terminal Tracking Cameras (TTCams) on the NASA Lucy Mission," Mar. 2024, 10.22541/essoar.171007074.47760362/v1.

[8] A. J. Liounis, C. Gnam, J. Swenson, K. Getzandanner, J. Small, and J. Lyzhoft, "The Goddard Image Analysis and Navigation Tool," January 2022.

[9] A. Liounis *et al.*, "Independent Optical Navigation Processing for the OSIRIS-REx Mission Using the Goddard Image Analysis and Navigation Tool," 2nd Space Imaging Workshop, 2019.

[10] "Camera Calibration and 3D Reconstruction," *OpenCV Dev Team*, 2014.

[11] A. J. Liounis, J. L. Small, J. C. Swenson, J. R. Lyzhoft, B. W. Ashman, K. M. Getzandanner, M. C. Moreau, C. D. Adam, J. M. Leonard, D. S. Nelson, J. Y. Pelgrift, B. J. Bos, S. R. Chesley, C. W. Hergenrother, and D. S. Lauretta, "Autonomous Detection of Particles and Tracks in Optical Images," *Earth and Space Science*, Vol. 7, No. 8, 2020, p. e2019EA000843. e2019EA000843 10.1029/2019EA000843, https://doi.org/10.1029/2019EA000843.

[12] D. Lang, D. W. Hogg, K. Mierle, M. Blanton, and S. Roweis, "ASTROMETRY.NET: BLIND ASTROMETRIC CALIBRATION OF ARBITRARY ASTRONOMICAL IMAGES," *The Astronomical Journal*, Vol. 139, mar 2010, p. 1782, 10.1088/0004-6256/139/5/1782.